

Structural characterization of the candidate Weyl semimetal CeGaGe

Liam J. Scanlon,¹ Santosh Bhusal,¹ Christina M. Hoffmann,² Helen He,² Sean R. Parkin,³ Brennan J. Arnold,¹ and William J. Gannon¹

¹*Department of Physics and Astronomy, University of Kentucky, Lexington, KY 40506 USA*

²*Neutron Scattering Division, Oak Ridge National Laboratory, Oak Ridge, TN 37831 USA*

³*Department of Chemistry, University of Kentucky, Lexington, KY 40506 USA*

(Dated: December 9, 2024)

Weyl semimetals have a variety of intriguing physical properties, including topologically protected electronic states that coexist with conducting states. Possible exploitation of topologically protected states in a conducting material is promising for technological applications. Weyl semimetals that form in a non-centrosymmetric structure that also contain magnetic moments may host a variety of emergent phenomena that cannot be seen in magnetic, centrosymmetric Weyl materials. It can be difficult to distinguish definitively between a centrosymmetric structure and one of its non-centrosymmetric subgroups with standard powder X-ray diffractometers in cases where two atoms in the compound have nearly the same atomic number, as is the case for the candidate Weyl semimetal CeGaGe. In these cases, a careful single-crystal neutron diffraction experiment with high-angle reflections provides complimentary information to X-ray diffraction and definitively resolves any ambiguity between centrosymmetric and non-centrosymmetric crystal structures. Single-crystal neutron diffraction measurements on the candidate Weyl semimetal CeGaGe confirms that its structure is non-centrosymmetric, described by space group 109 ($I4_1md$) rather than the centrosymmetric space group 141 ($I4_1/amd$). There are many high-angle reflections in the data set that give clear, physically intuitive evidence that CeGaGe forms with $I4_1md$ symmetry since Bragg planes of these reflections can contain Ga with no Ge or vice versa whereas the Bragg planes for a structure with $I4_1/amd$ symmetry would have a mix of Ga and Ge. Further, in some crystals we have studied, there is clear evidence for a structural transition from body-centered $I4_1md$ symmetry to primitive $P4_3$ and/or $P4_1$ symmetry.

I. Introduction

The recent appreciation for the role of topology in condensed matter physics has driven the study of materials that host protected electronic states, due to their potential uses in next generation technologies [1–6]. Among bulk materials that potentially host such states, Weyl semimetals also feature conducting states in their bulk, allowing for the exploitation of both protected and conventional electronic states in future applications. For a Weyl semimetal to exist, there must be either ordered magnetic moments that break time reversal symmetry (TRS) [7] or broken inversion symmetry in the crystal structure [8]. When combined with spin-orbit coupling, these broken symmetries can lead to degenerate bands that are topologically protected with linear dispersions that mimic Weyl particles [4–6].

In some instances, materials with Weyl points in their band structures possess both magnetic moments that order, breaking TRS, and non-centrosymmetric crystal structures. In such materials, it is possible to have Weyl states above the magnetic ordering temperature and study the interplay of Weyl quasiparticles with magnetic ordering. One such family of materials with non-centrosymmetric crystal structures that have been studied in this context are the RXZ materials where R is a rare earth element, X is Al or Ga, and Z is Si or Ge. There are at least 12 known materials in this fam-

ily [8–59]. When the rare earth element is La, there are no magnetic moments and TRS is preserved [8, 35–37]. When the rare earth element is Ce, Pr, Nd, Sm, or Gd the materials order magnetically and break TRS below the ordering temperature [9–34, 38–59]. As single crystals, each member of this family has tetragonal, non-centrosymmetric $I4_1md$ symmetry (space group 109).

A wide variety of physics is found in this material family. For instance, in NdAlSi the ordered magnetic structure is helical, with an incommensurate ordering vector that matches the nesting of the Weyl nodes in the band structure [9]. In CeAlGe, the magnetic order is a long wavelength meron-antimeron type order, where the topology of the order can be tuned with magnetic field, while simultaneously changing the magnitude of the observed topological Hall effect [20]. In CeAlSi, the position of the Weyl nodes move in reciprocal space with the onset of magnetic order [32]. In PrAlSi, a magnetic field induced Lifshitz transition has been observed [51].

A number of these materials were first identified not as high-quality single crystals but rather in polycrystalline form. For example, CeAlGe and NdAlSi were both first produced as polycrystals via arc-melting [60–62]. In these instances, the materials were reported to be alloys, with symmetry given as $I4_1/amd$ (space group 141) based on powder X-ray diffraction (PXRD) measurements. The difference between $I4_1md$ and $I4_1/amd$

in the context of these materials is the positioning of the X and Z atoms in the structure. With non-centrosymmetric $I4_1md$ symmetry, the X and Z atoms occupy distinct crystallographic sites (with Wyckoff site symmetry 4a), shown in Fig. 1(a,c) for the material CeGaGe, the subject of this manuscript. With $I4_1/amd$ symmetry, the X and Z atoms would need to randomly occupy the same crystallographic site (with site symmetry 8e) with 50% occupancy, restoring inversion symmetry in the structure (Fig. 1(b,d)). In arc-melted samples, the random polycrystalline $I4_1md$ grains would be practically indistinguishable from an $I4_1/amd$ alloy in a PXRD experiment, especially due to the possibility of inversion twinning with the $I4_1md$ symmetry. Since the band structure in a material is intimately linked to the crystal structure, it is critical to have an accurate structure determined from high-quality single crystals to fully understand the emergent physics. In the case of CeAlGe, this was done with careful single-crystal X-ray diffraction (SCXRD) since the atomic scattering factors of Al and Ge are significantly different [17, 63]. For NdAlSi, a careful single-crystal neutron diffraction (SCND) experiment was performed due to the similarities in X-ray atomic scattering factor of Al and Si [9, 63].

The subject of this manuscript, CeGaGe, is also a member of the RXZ family. Early reports on arc-melted samples determined the crystal structure to have $I4_1/amd$ symmetry from PXRD [64, 65]. In CeGaGe, ferromagnetic order was seen at $T_C = 5.5$ K, with a Sommerfeld coefficient $\gamma = 40$ mJ/mol.K² [66], significantly larger than in CeAlGe ($\gamma = 0.93$ mJ/mol.K²) [17], suggesting enhanced electronic correlations. A more recent report on single crystals of CeGaGe grown from flux confirm the magnetic ordering at $T_C = 5.5$ K, but finds a considerably smaller Sommerfeld coefficient $\gamma = 13$ mJ/mol.K² [67]. All reports confirm that CeGaGe is a poor metal, with a residual resistivity ratio as high as 2 in the likely higher quality flux-grown crystals.

The central problem is that there has not yet been a definitive structural determination for CeGaGe. This is not possible using standard powder X-ray characterization tools available at most institutions. As discussed above, structural determination would not have been possible in early polycrystalline samples with PXRD. However, even a PXRD experiment on a sample made from crushed single crystals would struggle to determine the structure in the RXZ materials because of the random orientation of the powder grains. It was shown that PXRD data from flux-grown single crystals of CeGaGe fits well to a model with $I4_1md$ symmetry [67], but a side-by-side comparison of refinements to models with $I4_1md$ and $I4_1/amd$ symmetry has not been made. PXRD data collected from a sample made from crushed single crystals is shown in Fig. 2(a,b). Rietveld refinements [68] using models with $I4_1md$ (Fig. 2(a)) and $I4_1/amd$ (Fig. 2(b)) symmetry are virtually identical and give equivalently good descriptions of the data. This is discussed further

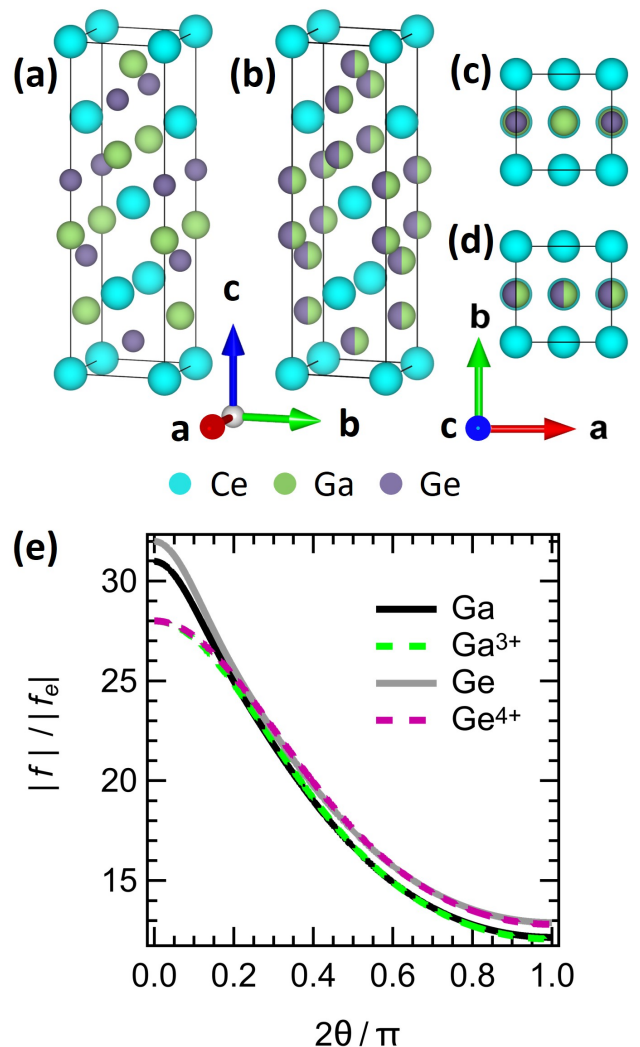


FIG. 1. Structure of CeGaGe: The unit cell of CeGaGe given $I4_1md$ (a) and $I4_1/amd$ (b) symmetries. Ce (cyan), Ga (green), and Ge (purple) are shown. For the $I4_1md$ space group, Ga and Ge occupy distinct crystallographic sites, each with Wyckoff symmetry 4a. For the $I4_1/amd$ space group, Ga and Ge are shown as a random mixture on the crystallographic site with Wyckoff symmetry 8e. Structures with the same $I4_1md$ (c) and $I4_1/amd$ (d) symmetries are shown projected along the crystal c -axis. (e) The normalized X-ray atomic scattering factors as a function of scattering angle 2θ are shown for elemental Ga (black solid line) and Ge (gray solid line) as well as the common Ga^{3+} (green dashed line), and Ge^{4+} (magenta dashed line) oxidation states calculated using the method prescribed by [63].

in section II. In CeGaGe specifically, SCXRD is complicated by the similarities of X-ray scattering factors for Ga and Ge. The X-ray scattering factors for Ga, Ge, and their common oxidation states are plotted in Fig. 1(e). There is little difference between Ga and Ge across 180° in scattering angle 2θ . A single-crystal structural determination avoiding the powder grain issue that also uses a complimentary technique to increase the contrast be-

tween the Ga and Ge sites would definitively determine the structure when combined with powder and single-crystal X-ray diffraction measurements that can be made at many institutions.

This same issue was faced with the material NdAlSi, where the similarity of Al and Si in XRD measurements made structural determination difficult, even with high-quality single crystals [9]. For that material, the structure was definitively determined to have $I4_1md$ symmetry using single-crystal neutron diffraction (SCND). Al and Si have significantly different coherent neutron scattering lengths [69, 70], making SCND a straightforward way to determine the structure.

We have performed a similar SCND experiment on CeGaGe as well as a number of single-crystal X-ray diffraction experiments. We find that the structure has $I4_1md$ symmetry in all samples. However, we also find in some samples that there is a subtle structural transition away from the body centered $I4_1md$ to the primitive, non-centrosymmetric $P4_3$ (and/or $P4_1$) symmetry upon decreasing temperature. These results lay a foundation for understanding the broader picture of magnetic and potential Weyl physics in CeGaGe and emphasizes that extreme caution in structural determination is needed in this family of materials.

II. Crystal Synthesis and Characterization

Elemental Ce (Aldrich 99.9%), Ga (Aesar 99.99999%), and Ge (Aldrich 99.999%) in the molar ratio 0.86 : 1.0 : 0.79 were arc-melted into two rods approximately 3 inches each in length. The melted material in each rod was cut, mixed, and remelted several times to ensure compositional homogeneity. These polycrystalline rods were then mounted and co-aligned in a Quantum Designs 2-mirror floating-zone furnace. floating-zone refinement was done under a 3 bar argon atmosphere to minimize loss of Ga and Ce due to their relatively high vapor pressures. While the crystal was being grown, there was a 4 standard cubic feet per hour flow of Ar through the system to minimize vapor plating to the walls of the growth chamber between the samples and mirrors. Growth was done at a rate of 8 mm/hour and each rod was rotated in opposite directions with a frequency of 5 rpm. This yielded a crystal of approximately 2.5 cm in length and 1.7 g in mass.

Energy dispersive X-ray spectroscopy (EDX) was used to determine composition of the sample. EDX spectra were taken at 38 sites on the sample using a Quanta FEG 250 environmental scanning electron microscope (SEM) equipped with an Oxford Instruments XSTREAM2 EDX detector. Each spectrum was collected with approximately 500,000 photon counts. A representative spectrum can be found in the supplementary information. Data were analyzed with the Oxford Instruments AZtec data suite using 20 keV range, 2048 channels, and pulse pile-up correction [71]. Carbon from the SEM mounting tape, aluminum from the interior of the SEM chamber,

Composition of $Ce_\alpha Ga_\beta Ge_\gamma$			
	α (Ce)	β (Ga)	γ (Ge)
EDX	0.95(2)	1.000(9)	0.86(1)
$I4_1md$	0.91(2)	1.00(2)	0.83(2)
$I4_1/amd$	0.93(4)	0.96(2)	1.00(8)

TABLE I. Composition of CeGaGe: The composition of the CeGaGe floating-zone refined crystal determined by EDX and by SCND refinements to models with $I4_1md$ and $I4_1/amd$ symmetry. The compositions from EDX data and refinement with the $I4_1md$ symmetry are within uncertainty of each other.

and any possible residual oxygen were included in fits to spectra, but not included in calculating molar compositions of the elements. Ce, Ga, and Ge showed molar ratio 0.95 : 1.0 : 0.86, as can be seen in table I. All spectra were normalized to a maximum composition of 1, with other compositions adjusted accordingly.

To confirm that models with $I4_1md$ and $I4_1/amd$ symmetry cannot be distinguished with powder X-ray diffraction tools, we performed an experiment using a powder prepared from the floating-zone refined crystal. Measurements were made with Bruker D8 Advance diffractometer equipped with a Göbel mirror and Soller slits for beam collimation and nickel filter to suppress K_β radiation. The results of the measurements are shown in Fig. 2. Rietveld refinements [68] to models with $I4_1md$ and $I4_1/amd$ symmetry using the FullProf Suite analysis package [72] are virtually identical. The reported χ^2 values are 1.05 for $I4_1md$ and 1.08 for $I4_1/amd$. The reliability factor R_{wp} was 18.7 for $I4_1md$ and 19.0 for $I4_1/amd$. Details of the refined structures can be seen in table S-I in the supplementary information.

III. SCND Data Acquisition and Analysis

A high-resolution neutron diffraction experiment with sufficient reciprocal space coverage can accurately determine whether CeGaGe has $I4_1md$ or $I4_1/amd$ symmetry. The bound coherent neutron scattering lengths for Ga and Ge differ by 12% [69, 70], making neutron scattering quite sensitive to differences in Ga and Ge. A single-crystal experiment eliminates the randomization of the crystal grains, while an experiment with large reciprocal space coverage can resolve features at particularly small length scales.

A SCND experiment was done using the TOPAZ diffractometer at the Spallation Neutron Source at Oak Ridge National Laboratory [73]. A crystal with mass 3.37 mg and roughly spherical shape with radius 0.3 mm cut from our floating-zone grown crystal was chosen for the experiment. The sample was mounted with random orientation onto an aluminum sample holder pin with glue, as is typical for TOPAZ experiments. The sample and pin were wrapped with pure Al foil to ensure good thermal contact and loaded into a closed cycle refrigerator on the instrument and cooled to $T = 100$ K. The

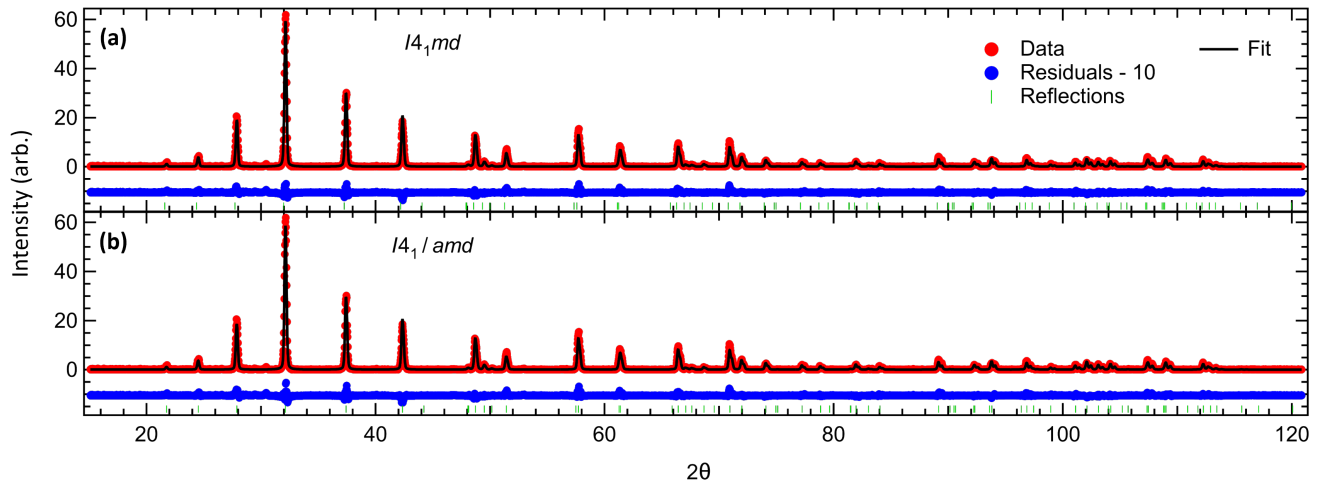


FIG. 2. Powder X-ray diffraction: Scattered X-ray intensity as a function of scattering angle 2θ measured by PXRD (red) and calculated by Rietveld refinements (black) to models with $I4_1md$ symmetry (a) and the $I4_1/amd$ symmetry (b). Refinements are nearly identical in both panels. Expected positions of Bragg reflections (green hatches) and offset residuals (blue) for each fit are shown. These refinements are virtually indistinguishable.

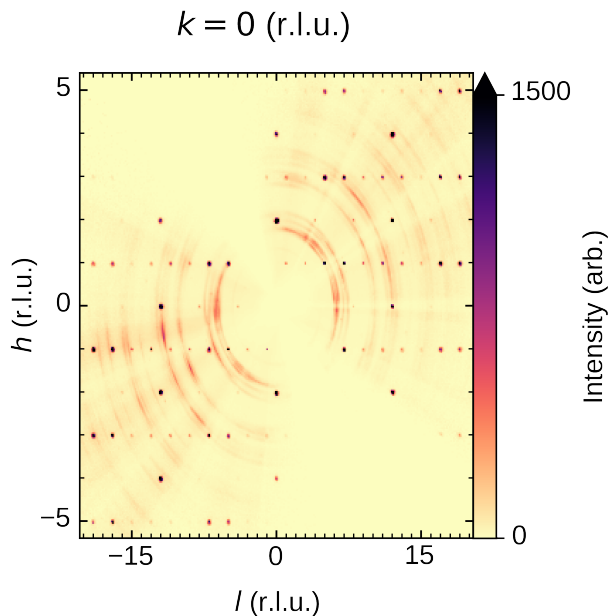


FIG. 3. The $k = 0$ plane of the merged SCND data before normalization. The data for the 19 different ϕ angles merged well, showing reflections only at integer indices in reciprocal space.

sample's orientation was varied by rotating around the vertical axis, and data were collected for 19 different rotation angles ϕ . At each angle, data were collected for approximately 50 minutes as the sample was exposed to a white beam of neutrons. The wavelengths of the scattered neutrons were resolved by time of flight (TOF).

From these measurements, the crystal unit cell was de-

termined to be tetragonal with $a = b = 4.2708(1)$ Å and $c = 14.5480(4)$ Å. All reciprocal space scattering data are indexed in reciprocal lattice units (r.l.u.). A representative plot of the data in the $k = 0$ reciprocal space plane is shown in Fig. 3. Measurements from all 19 rotation angles merged well and all diffraction peaks appear at integer reciprocal lattice indices, indicating a high-quality single-crystal sample. The $k = \pm 1$ planes are shown in figure S-3 of the supplementary information to further illustrate data quality.

The raw time-of-flight data were reduced using Mantid reduction scripts for TOPAZ measurements [74, 75]. The reduction normalizes the data, accounting for absorption, neutron flux, solid angle, Lorentz factor, background, and outliers. The reduced data give the structure factor for each observed Bragg reflection in arbitrary units. For both structures, 4430 Bragg reflections were indexed. Each of the structure factors had square modulus $|F_o|^2$ and uncertainty σ_o^2 such that $|F_o|^2/\sigma_o^2 \geq 3$, which is larger than the forced signal to noise cutoff of $|F_o|^2/\sigma_o^2 \geq 1$.

Structural refinement was performed using the General Structure Analysis System-II (GSASII) [76] software. Scale, atomic position, anisotropic thermal parameters, occupancy, and extinction were refined for models with $I4_1md$ and $I4_1/amd$ symmetry. When the refinement is carried out with site exchange in a model with $I4_1md$ symmetry, there is less than 3% site exchange between Ga and Ge, with uncertainty on the order 10%, and so the crystallographic information reported here is from a refinement that does not include site exchange. Calculated structure factors using both the $I4_1md$ and $I4_1/amd$ space groups agree reasonably well with observed structure factors, as can be seen in Fig. 4(a,c). When $|F_o|^2$

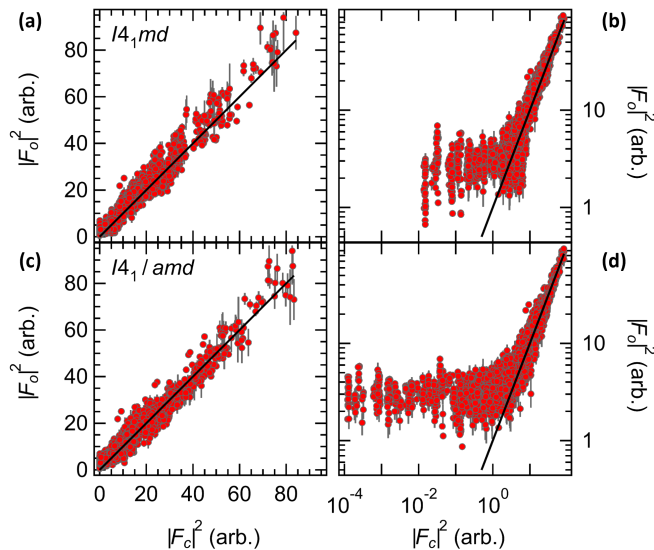


FIG. 4. SCND refinements: Square moduli of observed versus square moduli of calculated structure factors for space groups $I4_1md$ (a) and $I4_1/amd$ (c). The solid black lines have slope 1 and pass through the origin. Plots (b) and (d) are the same plots as (a) and (c) respectively, but on a log-log scale.

is plotted as a function of the refined, calculated structure factors $|F_c|^2$, in both models the result is a data set that is tightly grouped to a line of slope 1 passing through the origin, indicating that the refinements $|F_c|^2$ are good descriptions of our observation $|F_o|^2$. Indeed, for the strongest reflections, there is little difference between the two crystal structures in question.

However, the reliability factors (R) for the two structural models are significantly different, where R is given by

$$R = \frac{\sum | |F_o| - |F_c| |}{\sum |F_o|} \quad (1)$$

where F_o and F_c are the observed and calculated structure factors respectively. $R = 0.161$ for $I4_1md$ and $R = 0.224$ for $I4_1/amd$, suggesting that $I4_1md$ is a significantly better description of the measurements. The goodness-of-fit value of 19.13 for $I4_1md$ is lower than the goodness-of-fit value of 22.40 for $I4_1/amd$. The main difference in the refinements for the two structural models is seen in the weakest Bragg reflections. When the same data from Figures 4(a,c) are plotted on a log-log scale to emphasize the weakest reflections (Fig. 4(b,d)), it is clear that there are a number of peaks that are not well described by a model with $I4_1/amd$ symmetry.

This is not simply an artifact of plotting on a log-log scale. There are 1236 data points where $10^{-4} \leq |F_c|^2 \leq 1.25$ for the $I4_1/amd$ space group. Each of these reflections in the $I4_1/amd$ data set indexed by h , k , l with rotation angle ϕ , can be plotted against the corresponding reflection in the $I4_1md$ data set indexed by the same h , k , l , and ϕ . For 986 of the 1236 reflections,

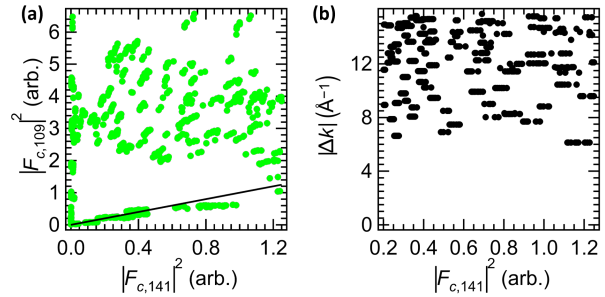


FIG. 5. Reflections with small $|F_c|^2$: (a) $|F_c|^2$ for the $I4_1md$ space group versus corresponding $|F_c|^2$ for $I4_1/amd$ for common Bragg reflections appearing at the same ϕ . The black line has a slope of 1 and passes through the origin. (b) Magnitude of scattering vector as a function of $|F_c|^2$ for $I4_1/amd$.

$I4_1md$ predicts more intensity than $I4_1/amd$, putting 911 of the 1236 measured $|F_o|^2$ in better agreement with the $I4_1md$ structural model.

The scattering vectors for these 1236 data points have relatively large magnitudes, as can be seen in Fig. 5(b). Since magnitudes in reciprocal space are generally inversely proportional to magnitudes in real space, this suggests that the reflections where $I4_1md$ provides a significantly better description are representative of structure at short length scale. Indeed, the distance between Ga and its nearest neighbor Ge is 2.417 Å, which is a short length scale.

Closer examination of these reflections reveals how important they are in the structural determination. Example Bragg planes for one of the reflections in Fig. 5, the $(-2, -2, -16)$ peak, can be seen in Fig. 6(a), along with a plot of the $(-2, -2, -16)$ peak in reciprocal space, Fig. 6(b). Although this is a weak peak, it has good signal to noise and is considerably stronger than the Al background that surrounds it. Considering that the Bragg plane for $(-2, -2, -16)$ can have Ga atoms with no Ge atoms or vice versa for the $I4_1md$ space group, but would include both Ga and Ge for $I4_1/amd$, it is physically intuitive why the intensities of these peaks are predicted to be significantly lower for the $I4_1/amd$ model. A common feature of the data points in Fig. 5 is that they appear at relatively large scattering vectors and come from Bragg planes that would contain only Ga or Ge for $I4_1md$, but would contain a mix of Ga and Ge for $I4_1/amd$.

All of the refined quantities for the correct $I4_1md$ model except for the scale factors are shown in Table II. The unit cell parameters are in excellent agreement with previous reports [64, 65, 67]. The average of the anisotropic thermal parameters is smaller than the isotropic thermal parameters reported by reference [64]. This is expected, given that the present experiment was done at $T = 100$ K while the experiment in reference [64] was done at room temperature.

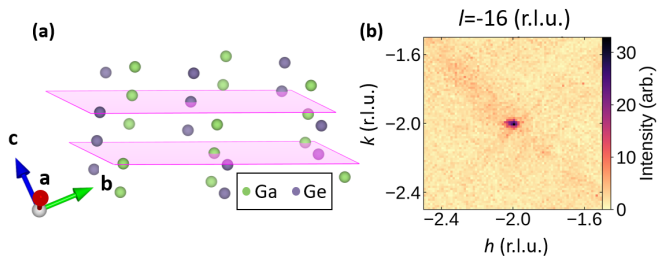


FIG. 6. (a) The crystal structure with $I4_1md$ symmetry without Ce atoms, showing Ga in green and Ge in purple. Lattice planes with indices $(-2, -2, -16)$, corresponding to one of the Bragg reflections where the structure factors for the $I4_1md$ and $I4_1/amd$ models differ most, are shown. (b) Plot of the $(-2, -2, -16)$ peak in reciprocal space, indicating that although a weak reflection, it is clearly distinguishable from the background scattering.

Atom	x	y	z	occ.
Ce	0.0	0.0	0.000	0.91(2)
Ga	0.0	0.0	0.4171(1)	1.00(2)
Ge	0.0	0.0	0.5829(1)	0.83(2)

Atom	$U_{1,1}$	$U_{2,2}$	$U_{3,3}$
Ce	0.0038(8)	0.010(1)	0.0077(7)
Ga	0.0031(3)	0.0146(7)	0.0011(4)
Ge	0.019(1)	0.019(1)	0.013(1)

TABLE II. Crystallographic information of the CeGaGe structure for $I4_1md$ refinement: The anisotropic thermal parameter $U_{1,1}$ is proportional to the mean square displacement of the atom along the a -axis, $U_{2,2}$ is proportional to the mean square displacement of the atom along the b -axis, and $U_{3,3}$ is proportional to the mean square displacement along the c -axis. The secondary type-1 extinction parameter E_g was 5.22×10^{-4} .

IV. Single-Crystal X-Ray Diffraction

A complimentary single-crystal X-ray scattering measurement can give further structural information, especially since Friedel's law prevents observation of inversion twinning without resonant scattering and none of the elements in CeGaGe have resonant effects in the thermal neutron range [77, 78]. The only merohedric twin law allowed for $I4_1md$ is inversion twinning, which is distinguishable in a SCXRD experiment due to resonant scattering of electrons. Moreover, the relative ease of a SCXRD experiment in a local laboratory would allow for far more rapid structural analysis of new samples grown under different conditions going forward.

A small grain of the sample used for SCND was used to conduct a SCXRD experiment. Data were collected at $T = 100$ K on a Bruker D8 Venture κ -axis diffractometer using molybdenum K_α X-rays with nitrogen gas stream for cooling. Raw data were integrated, scaled, merged and corrected for Lorentz-polarization effects using the APEX3 package [79]. Corrections for absorption were

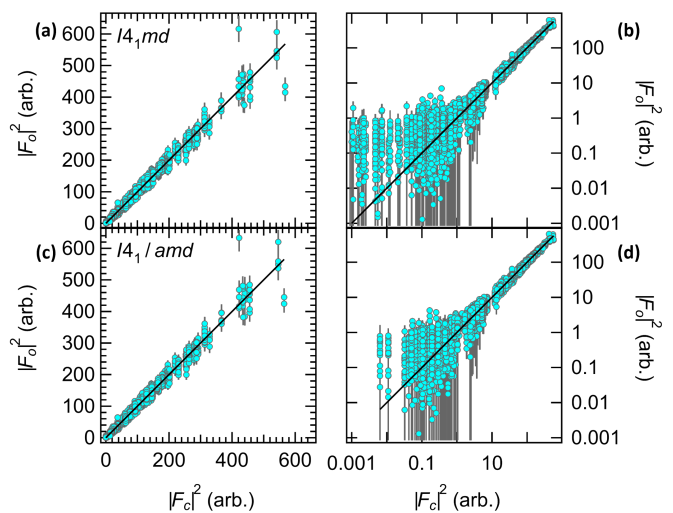


FIG. 7. Square moduli of observed structure factors measured with SCXRD versus square moduli of calculated structure factors for space groups $I4_1md$ (a) and $I4_1/amd$ (c). Solid black lines have slope 1 and pass through the origin. Plots (b) and (d) are the same plots as (a) and (c) respectively, but on a log-log scale. There are 181 data points where $0.001 < |F_c|^2 < 0.0064$ for $I4_1md$. For each of these 181 data points, all data points with matching h, k, l indices for the $I4_1/amd$ data set have $|F_c|^2 = 0$.

applied using SADABS [80]. The structure was solved by iterative dual-space methods (SHELXT, [81]) and refinement was carried out against square moduli of observed structure factors by weighted full-matrix least-squares (SHELXL, [82]). All atoms were refined with anisotropic displacement parameters. Crystallographic parameters of the determined structure are summarized in Table S-II of the supplementary information.

The crystallographic reliability factors, defined by equation 1, are superior for refinements using $I4_1md$ versus $I4_1/amd$ symmetries, giving $R = 0.0249$ for $I4_1md$ and $R = 0.0263$ for $I4_1/amd$. The goodness-of-fit values are 1.146 for $I4_1md$ and 1.258 for $I4_1/amd$.

Given all of these results, $I4_1md$ symmetry is clearly the correct description for this CeGaGe sample. Analysis of the SCXRD data with this symmetry give a Flack parameter [83] of 0.49(8). The small uncertainty of the Flack parameter indicates that the parameter is well defined and so the structure is non-centrosymmetric. The Flack parameter being close to 0.5 indicates that there is nearly perfect inversion twinning in the sample.

These SCXRD results are plotted in Fig. 7 in a fashion similar to the SCND presentation (Fig. 4). The discrepancies between data and refinements in Fig. 7(b, d) are not nearly as pronounced as they are in the the SCND analysis, Figs. 4(b, d). When combined, SCND and SCXRD give a more complete picture of the crystal structure of CeGaGe.

V. Structural phase transition in other CeGaGe samples

Given the relative scarcity of neutron scattering time on a high-resolution diffractometer and reasonable agreement between our SCND and SCXRD results, SCXRD was used to determine the structure of additional CeGaGe crystals. As discussed above, the crystal that was used on the TOPAZ diffractometer was found to have the I -centered $I4_1md$ tetragonal symmetry at $T = 100$ K in the SCND experiment and at $T = 100$ K in the SCXRD experiment. Additional SCXRD measurements confirm that this is the correct symmetry at room temperature for this sample.

However, a crystal synthesized using the flux-growth technique [84, 85] using the same recipe as [67] shows a transition from I -centered to a primitive tetragonal symmetry as can be seen in figure 8. When this sample is measured with SCXRD at room temperature, all Bragg reflections that are observed can be indexed with reflections that are expected for $I4_1md$ symmetry. As an example, the $k = 1$ Bragg plane is shown in Fig. 8(a), where only expected reflections are observed. When the sample is cooled to $T = 100$ K and the measurement is repeated (Fig. 8(b)), weak Bragg reflections appear that are not allowed for $I4_1md$ symmetry. These additional reflections are consistent with a transition to a primitive tetragonal structure.

SCXRD refinement shows that the structure of the flux-grown sample is well described with chiral $P4_3$ symmetry (space group 78). A Flack parameter of 0.44(8), indicates a mix of $P4_3$ and its enantiomer $P4_1$ (space group 76) since point inversion of a chiral structure transforms it to its enantiomer [86, 87]. Crystallographic information for the refinement to the $P4_3$ structure can be found in table S-III of the supplementary information.

The difference between $I4_1md$ and $P4_3$ (or $P4_1$) is extremely subtle in this context. Given that it occurs at a temperature between room temperature and $T = 100$ K, the thermodynamic signature of such a minor movement of the atoms would be virtually impossible to resolve using typical lab-based physical property probes such as specific heat. A more precise measurement of one of the elastic properties of the crystal would be needed to find the precise temperature of the phase transition or if the transition is continuous.

Since we have demonstrated that it is possible to synthesize CeGaGe crystals that remain in the body-centered structure down to 100 K using float zone refining, we can speculate that the structural transition observed in the flux-grown crystals is either due to small amounts of impurities or crystallographic defects in the flux-grown samples. Given the dependence on the physical properties of CeAlGe to precise stoichiometry [17, 24, 61, 88], minor compositional variations could also be responsible for the symmetry change upon lowering

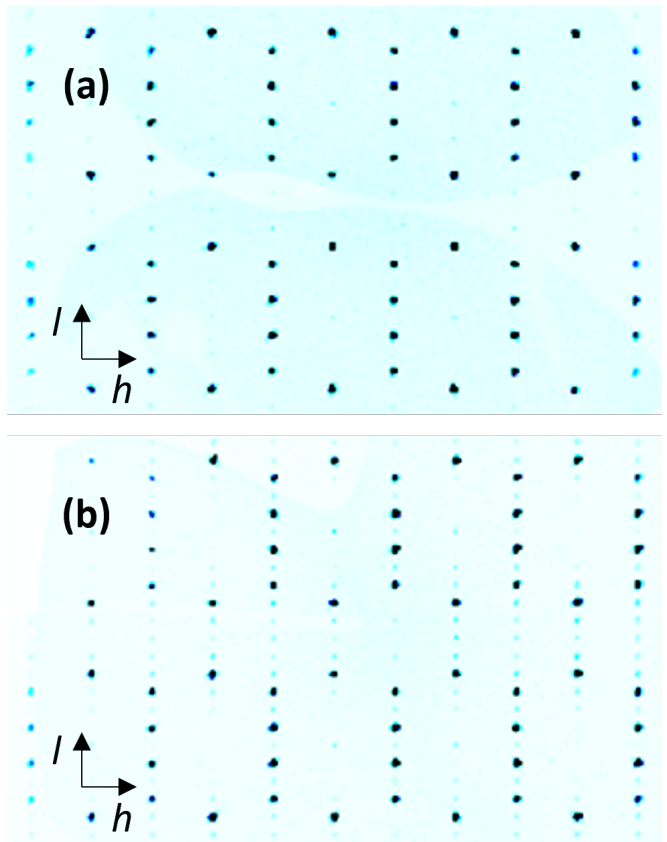


FIG. 8. Evidence of structural transition in flux-grown CeGaGe obtained with SCXRD. (a) the $k = 1$ plane at room temperature. Intensity is on a linear scale and contrast has been enhanced to show weaker peaks more clearly. The l -axis is vertical and the h -axis is horizontal. (b) the $k = 1$ plane at 100 K. The appearance of additional weak peaks indicates that the structure has transitioned from the body-centered tetragonal $I4_1md$ structure to the primitive tetragonal $P4_1$ or $P4_3$ structure.

temperature.

VI. Conclusion

The measurements presented in this manuscript definitively show that the candidate Weyl semimetal CeGaGe crystallizes with non-centrosymmetric $I4_1md$ symmetry at room temperature and in some samples, remains in this symmetry at cryogenic temperatures. For those samples that show a structural transition, it is a transition to a another non-centrosymmetric symmetry. Given its compositional and structural similarities to other materials that host an interplay between exotic electronic states and magnetism, CeGaGe is an excellent candidate for study in this context.

The strong magnetic anisotropy and possible signatures of multiple magnetic phases seen in measurements of the magnetic susceptibility in flux-grown crystals [67] suggest that it is likely that there will be rich magnetic phenomena in CeGaGe, which can now be understood

definitively with respect to the crystal structure. Given the strong sensitivity of the physical properties to precise stoichiometry in related CeAlGe [24] and the structural transitions discussed in section V, caution should be used in interpreting CeGaGe measurements. How-

ever now that the structure is known, any future measurements and calculations of electronic structure are on much firmer footing both in the broad context of magnetic Weyl semimetals and in the narrower context of CeGaGe specifically.

-
- [1] M. Z. Hasan and C. L. Kane, *Rev. Mod. Phys.* **82**, 3045 (2010).
- [2] A. H. Castro Neto, F. Guinea, N. M. R. Peres, K. S. Novoselov, and A. K. Geim, *Rev. Mod. Phys.* **81**, 109 (2009).
- [3] E. Y. Andrei and A. H. MacDonald, *Nature Materials* **19**, 1265–1275 (2020).
- [4] B. Yan and C. Felser, *Annual Review of Condensed Matter Physics* **8**, 337–354 (2017).
- [5] M. Z. Hasan, G. Chang, I. Belopolski, G. Bian, S.-Y. Xu, and J.-X. Yin, *Nature Reviews Materials* **6**, 784–803 (2021).
- [6] N. P. Armitage, E. J. Mele, and A. Vishwanath, *Rev. Mod. Phys.* **90**, 015001 (2018).
- [7] I. Belopolski, K. Manna, D. S. Sanchez, G. Chang, B. Ernst, J. Yin, S. S. Zhang, T. Cochran, N. Shumiya, H. Zheng, B. Singh, G. Bian, D. Multer, M. Litskevich, X. Zhou, S.-M. Huang, B. Wang, T.-R. Chang, S.-Y. Xu, A. Bansil, C. Felser, H. Lin, and M. Z. Hasan, *Science* **365**, 1278–1281 (2019).
- [8] S.-Y. Xu, N. Alidoust, G. Chang, H. Lu, B. Singh, I. Belopolski, D. S. Sanchez, X. Zhang, G. Bian, H. Zheng, M.-A. Husanu, Y. Bian, S.-M. Huang, C.-H. Hsu, T.-R. Chang, H.-T. Jeng, A. Bansil, T. Neupert, V. N. Strocov, H. Lin, S. Jia, and M. Z. Hasan, *Science Advances* **3**, e1603266 (2017), <https://www.science.org/doi/pdf/10.1126/sciadv.1603266>.
- [9] J. Gaudet, H.-Y. Yang, S. Baidya, B. Lu, G. Xu, Y. Zhao, J. A. Rodriguez-Rivera, C. M. Hoffmann, D. E. Graf, D. H. Torchinsky, P. Nikolić, D. Vanderbilt, F. Tafti, and C. L. Broholm, *Nat. Mater.* **20**, 1650 (2021).
- [10] J.-F. Wang, Q.-X. Dong, Z.-P. Guo, M. Lv, Y.-F. Huang, J.-S. Xiang, Z.-A. Ren, Z.-J. Wang, P.-J. Sun, G. Li, and G.-F. Chen, *Phys. Rev. B* **105**, 144435 (2022).
- [11] J.-F. Wang, Q.-X. Dong, Y.-F. Huang, Z.-S. Wang, Z.-P. Guo, Z.-J. Wang, Z.-A. Ren, G. Li, P.-J. Sun, X. Dai, and G.-F. Chen, *Physical Review B* **108**, 10.1103/physrevb.108.024423 (2023).
- [12] C. Li, J. Zhang, Y. Wang, H. Liu, Q. Guo, E. Rienks, W. Chen, F. Bertran, H. Yang, D. Phuyal, H. Fedderwitz, B. Thiagarajan, M. Dendzik, M. H. Berntsen, Y. Shi, T. Xiang, and O. Tjernberg, *Nature Communications* **14**, 10.1038/s41467-023-42996-8 (2023).
- [13] P. K. Tanwar, M. Ahmad, M. S. Alam, X. Yao, F. Tafti, and M. Matusiak, *Phys. Rev. B* **108**, L161106 (2023).
- [14] Q.-X. Dong, J.-F. Wang, L.-B. Zhang, J.-L. Bai, Q.-Y. Liu, J.-W. Cheng, P.-Y. Liu, C.-D. Li, J.-S. Xiang, Z.-A. Ren, P.-J. Sun, and G.-F. Chen, *Phys. Rev. B* **108**, 205143 (2023).
- [15] K. Cho, W. H. Shon, K. Kim, J. Bae, J. Lee, C.-S. Park, S. Yoon, B. Cho, P. Rawat, and J.-S. Rhyee, *SSRN Electronic Journal* 10.2139/ssrn.4217268 (2022).
- [16] X. He, Y. Li, H. Zeng, Z. Zhu, S. Tan, Y. Zhang, C. Cao, and Y. Luo, *Science China Physics, Mechanics & Astronomy* **66**, 10.1007/s11433-022-2051-4 (2023).
- [17] H. Hodovanets, C. J. Eckberg, P. Y. Zavalij, H. Kim, W.-C. Lin, M. Zic, D. J. Campbell, J. S. Higgins, and J. Paglione, *Phys. Rev. B* **98**, 245132 (2018).
- [18] H. Hodovanets, C. J. Eckberg, D. J. Campbell, Y. Eo, P. Y. Zavalij, P. Piccoli, T. Metz, H. Kim, J. S. Higgins, and J. Paglione, *Phys. Rev. B* **106**, 235102 (2022).
- [19] M. M. Piva, J. C. Souza, G. A. Lombardi, K. R. Pakuszewski, C. Adriano, P. G. Pagliuso, and M. Nicklas, *Physical Review Materials* **7**, 10.1103/physrevmaterials.7.074204 (2023).
- [20] P. Puphal, V. Pomjakushin, N. Kanazawa, V. Ukleev, D. J. Gawryluk, J. Ma, M. Naamneh, N. C. Plumb, L. Keller, R. Cubitt, E. Pomjakushina, and J. S. White, *Phys. Rev. Lett.* **124**, 017202 (2020).
- [21] T. Suzuki, L. Savary, J.-P. Liu, J. W. Lynn, L. Balents, and J. G. Checkelsky, *Science* **365**, 377 (2019), <https://www.science.org/doi/pdf/10.1126/science.aat0348>.
- [22] N. C. Drucker, T. Nguyen, F. Han, P. Siriviboon, X. Luo, N. Andrejevic, Z. Zhu, G. Bednik, Q. T. Nguyen, Z. Chen, L. K. Nguyen, T. Liu, T. J. Williams, M. B. Stone, A. I. Kolesnikov, S. Chi, J. Fernandez-Baca, C. S. Nelson, A. Alatas, T. Hogan, A. A. Puretzy, S. Huang, Y. Yu, and M. Li, *Nature Communications* **14**, 10.1038/s41467-023-40765-1 (2023).
- [23] Z. Wang, X. He, F. Lu, H. Zeng, S. Zou, X.-X. Zhang, and Y. Luo, *Phys. Rev. B* **109**, 245106 (2024).
- [24] P. Puphal, C. Mielke, N. Kumar, Y. Soh, T. Shang, M. Medarde, J. S. White, and E. Pomjakushina, *Physical Review Materials* **3**, 10.1103/physrevmaterials.3.024204 (2019).
- [25] M. S. Alam, A. Fakhredine, M. Ahmad, P. K. Tanwar, H.-Y. Yang, F. Tafti, G. Cuono, R. Islam, B. Singh, A. Lynnyk, C. Autieri, and M. Matusiak, *Physical Review B* **107**, 10.1103/physrevb.107.085102 (2023).
- [26] C. Tzschaschel, J.-X. Qiu, X.-J. Gao, H.-C. Li, C. Guo, H.-Y. Yang, C.-P. Zhang, Y.-M. Xie, Y.-F. Liu, A. Gao, D. Bérubé, T. Dinh, S.-C. Ho, Y. Fang, F. Huang, J. Nordlander, Q. Ma, F. Tafti, P. J. W. Moll, K. T. Law, and S.-Y. Xu, *Nature Communications* **15**, 10.1038/s41467-024-47291-8 (2024).
- [27] E. Cheng, L. Yan, X. Shi, R. Lou, A. Fedorov, M. Behnami, J. Yuan, P. Yang, B. Wang, J.-G. Cheng, Y. Xu, Y. Xu, W. Xia, N. Pavlovskii, D. C. Peets, W. Zhao, Y. Wan, U. Burkhardt, Y. Guo, S. Li, C. Felser, W. Yang, and B. Büchner, *Nature Communications* **15**, 10.1038/s41467-024-45658-5 (2024).
- [28] M. M. Piva, J. C. Souza, V. Brousseau-Couture, S. Sorn, K. R. Pakuszewski, J. K. John, C. Adriano, M. Côté, P. G. Pagliuso, A. Paramekanti, and M. Nicklas, *Physical Review Research* **5**, 10.1103/physrevresearch.5.013068 (2023).
- [29] A. P. Sakhya, C.-Y. Huang, G. Dhakal, X.-J. Gao, S. Regmi, B. Wang, W. Wen, R.-H. He, X. Yao, R. Smith,

- M. Sprague, S. Gao, B. Singh, H. Lin, S.-Y. Xu, F. Tafti, A. Bansil, and M. Neupane, *Phys. Rev. Mater.* **7**, L051202 (2023).
- [30] Y. Sun, C. Lee, H.-Y. Yang, D. H. Torchinsky, F. Tafti, and J. Orenstein, *Phys. Rev. B* **104**, 235119 (2021).
- [31] B. Xu, J. Franklin, A. Jayakody, H. Yang, F. Tafti, and I. Sochnikov, *Advanced Quantum Technologies* **4**, 10.1002/qute.202000101 (2021).
- [32] H.-Y. Yang, B. Singh, J. Gaudet, B. Lu, C.-Y. Huang, W.-C. Chiu, S.-M. Huang, B. Wang, F. Bahrami, B. Xu, J. Franklin, I. Sochnikov, D. E. Graf, G. Xu, Y. Zhao, C. M. Hoffman, H. Lin, D. H. Torchinsky, C. L. Broholm, A. Bansil, and F. Tafti, *Phys. Rev. B* **103**, 115143 (2021).
- [33] A. Laha, A. K. Kundu, N. Aryal, E. S. Bozin, J. Yao, S. Paone, A. Rajapitamahuni, E. Vescovo, T. Valla, M. Abeykoon, R. Jing, W. Yin, A. N. Pasupathy, M. Liu, and Q. Li, *Phys. Rev. B* **109**, 035120 (2024).
- [34] P. Meena, A. Choudhury, M. Mudgal, S. Bagga, V. K. Tiwari, S. Rajput, C. S. Yadav, V. K. Malik, T. Maitra, and J. Nayak, *Journal of Physics: Condensed Matter* **10.1088/1361-648x/ad912e** (2024).
- [35] W. Cao, N. Zhao, C. Pei, Q. Wang, Q. Zhang, T. Ying, Y. Zhao, L. Gao, C. Li, N. Yu, L. Gu, Y. Chen, K. Liu, and Y. Qi, *Phys. Rev. B* **105**, 174502 (2022).
- [36] T. Ng, Y. Luo, J. Yuan, Y. Wu, H. Yang, and L. Shen, *Phys. Rev. B* **104**, 014412 (2021).
- [37] I. Kim, B. Kang, H. Kim, and M. Choi, *Phys. Rev. Mater.* **8**, 054203 (2024).
- [38] C. Dhital, R. L. Dally, R. Ruvalcaba, R. Gonzalez-Hernandez, J. Guerrero-Sanchez, H. B. Cao, Q. Zhang, W. Tian, Y. Wu, M. D. Frontzek, S. K. Karna, A. Meads, B. Wilson, R. Chapai, D. Graf, J. Bacsá, R. Jin, and J. F. DiTusa, *Phys. Rev. B* **107**, 224414 (2023).
- [39] N. Kikugawa, T. Terashima, T. Kato, M. Hayashi, H. Yamaguchi, and S. Uji, *Inorganics* **11**, 20 (2023).
- [40] T. Wang, Y. Guo, C. Wang, and S. Yang, *Solid State Communications* **321**, 114041 (2020).
- [41] H.-Y. Yang, J. Gaudet, R. Verma, S. Baidya, F. Bahrami, X. Yao, C.-Y. Huang, L. DeBeer-Schmitt, A. A. Aczel, G. Xu, H. Lin, A. Bansil, B. Singh, and F. Tafti, *Phys. Rev. Mater.* **7**, 034202 (2023).
- [42] J. Zhao, W. Liu, A. Rahman, F. Meng, L. Ling, C. Xi, W. Tong, Y. Bai, Z. Tian, Y. Zhong, Y. Hu, L. Pi, L. Zhang, and Y. Zhang, *New Journal of Physics* **24**, 013010 (2022).
- [43] N. Kikugawa, S. Uji, and T. Terashima, *Phys. Rev. B* **109**, 035143 (2024).
- [44] D. Destraz, L. Das, S. S. Tsirkin, Y. Xu, T. Neupert, J. Chang, A. Schilling, A. G. Grushin, J. Kohlbrecher, L. Keller, P. Puphal, E. Pomjakushina, and J. S. White, *npj Quantum Materials* **5**, 10.1038/s41535-019-0207-7 (2020).
- [45] B. Meng, H. Wu, Y. Qiu, C. Wang, Y. Liu, Z. Xia, S. Yuan, H. Chang, and Z. Tian, *APL Materials* **7**, 051110 (2019), https://pubs.aip.org/aip/apm/article-pdf/doi/10.1063/1.5090795/14562139/051110_1.online.pdf.
- [46] D. S. Sanchez, G. Chang, I. Belopolski, H. Lu, J.-X. Yin, N. Alidoust, X. Xu, T. A. Cochran, X. Zhang, Y. Bian, S. S. Zhang, Y.-Y. Liu, J. Ma, G. Bian, H. Lin, S.-Y. Xu, S. Jia, and M. Z. Hasan, *Nature Communications* **11**, 10.1038/s41467-020-16879-1 (2020).
- [47] R. Yang, M. Corasaniti, C. C. Le, C. Yue, Z. Hu, J. P. Hu, C. Petrovic, and L. Degiorgi, *npj Quantum Materials* **7**, 10.1038/s41535-022-00507-w (2022).
- [48] K. Shoriki, K. Moriishi, Y. Okamura, K. Yokoi, H. Usui, H. Murakawa, H. Sakai, N. Hanasaki, Y. Tokura, and Y. Takahashi, *Proceedings of the National Academy of Sciences* **121**, 10.1073/pnas.2316910121 (2024).
- [49] H.-Y. Yang, B. Singh, B. Lu, C.-Y. Huang, F. Bahrami, W.-C. Chiu, D. Graf, S.-M. Huang, B. Wang, H. Lin, D. Torchinsky, A. Bansil, and F. Tafti, *APL Materials* **8**, 011111 (2020), https://pubs.aip.org/aip/apm/article-pdf/doi/10.1063/1.5132958/13258871/011111_1.online.pdf.
- [50] M. Lyu, J. Xiang, Z. Mi, H. Zhao, Z. Wang, E. Liu, G. Chen, Z. Ren, G. Li, and P. Sun, *Phys. Rev. B* **102**, 085143 (2020).
- [51] L. Wu, S. Chi, H. Zuo, G. Xu, L. Zhao, Y. Luo, and Z. Zhu, *npj Quantum Materials* **8**, 10.1038/s41535-023-00537-y (2023).
- [52] R. Lou, A. Fedorov, L. Zhao, A. Yaresko, B. Büchner, and S. Borisenko, *Physical Review B* **107**, 10.1103/physrevb.107.035158 (2023).
- [53] X. Yao, J. Gaudet, R. Verma, D. E. Graf, H.-Y. Yang, F. Bahrami, R. Zhang, A. A. Aczel, S. Subedi, D. H. Torchinsky, J. Sun, A. Bansil, S.-M. Huang, B. Singh, P. Blaha, P. Nikolić, and F. Tafti, *Phys. Rev. X* **13**, 011035 (2023).
- [54] W. Cao, Y. Su, Q. Wang, C. Pei, L. Gao, Y. Zhao, C. Li, N. Yu, J. Wang, Z. Liu, Y. Chen, G. Li, J. Li, and Y. Qi, *Chinese Physics Letters* **39**, 047501 (2022).
- [55] L. Xu, H. Niu, Y. Bai, H. Zhu, S. Yuan, X. He, Y. Han, L. Zhao, Y. Yang, Z. Xia, Q. Liang, and Z. Tian, *Journal of Physics: Condensed Matter* **34**, 485701 (2022).
- [56] J. Gong, H. Wang, K. Han, X.-Y. Zeng, X.-P. Ma, Y.-T. Wang, J.-F. Lin, X.-Y. Wang, and T.-L. Xia, *Phys. Rev. B* **109**, 024434 (2024).
- [57] H. Lu, W. Yang, Y. Huang, Y. Bian, X. Zhang, and S. Jia, *Materials Letters* **335**, 133819 (2023).
- [58] J. Bouaziz, G. Bihlmayer, C. E. Patrick, J. B. Staunton, and S. Blügel, *Phys. Rev. B* **109**, L201108 (2024).
- [59] H. Lu, H. Zang, X. Ren, X. He, V. Rodionova, E. Yan, and K. Magomedov, *Journal of Materials Science* **59**, 14653–14660 (2024).
- [60] J. T. Zhao and E. Parthé, *Acta Crystallographica Section C Crystal Structure Communications* **46**, 2276–2279 (1990).
- [61] S. Dhar, S. Pattalwar, and R. Vijayaraghavan, *Journal of Magnetism and Magnetic Materials* **104–107**, 1303 (1992), proceedings of the International Conference on Magnetism, Part II.
- [62] W. He, J. Zhang, L. Zeng, and Y. Zhuang, *Rare Metals* **25**, 355–358 (2006).
- [63] P. J. Brown, A. G. Fox, E. N. Maslen, M. A. O’Keefe, and B. T. M. Willis, *Intensity of diffracted intensities, in International Tables for Crystallography* (International Union of Crystallography, 2006) p. 554–595.
- [64] Y. Grin, P. Rogl, B. Chevalier, A. Fedorchuk, and I. Gryniv, *Journal of the Less Common Metals* **167**, 365 (1991).
- [65] R. Pöttgen and B. Chevalier, *Zeitschrift für Naturforschung B* **70**, 695 (2015).
- [66] S. Dhar, S. Pattalwar, and R. Vijayaraghavan, *Physica B: Condensed Matter* **186–188**, 491–493 (1993).
- [67] D. Ram, S. Malick, Z. Hossain, and D. Kaczorowski, *Phys. Rev. B* **108**, 024428 (2023).
- [68] H. M. Rietveld, *Journal of Applied Crystallography* **2**, 65–71 (1969).
- [69] V. F. Sears, *Neutron News* **3**, 26 (1992),

- <https://doi.org/10.1080/10448639208218770>.
- [70] Neutron scattering lengths and cross sections — ncnr.nist.gov, <https://www.ncnr.nist.gov/resources/n-lengths/> (2021), [Accessed 16-07-2024].
- [71] P. Statham, *Microscopy and Microanalysis* **13**, 1428 (2007), <https://academic.oup.com/mam/article-pdf/13/S02/1428/48134251/mam1428.pdf>.
- [72] J. Rodríguez-Carvajal, *Physica B: Condensed Matter* **192**, 55–69 (1993).
- [73] L. Coates, H. B. Cao, B. C. Chakoumakos, M. D. Frontzek, C. Hoffmann, A. Y. Kovalevsky, Y. Liu, F. Meilleur, A. M. dos Santos, D. A. A. Myles, X. P. Wang, and F. Ye, *Review of Scientific Instruments* **89**, 10.1063/1.5030896 (2018).
- [74] F. Akeroyd, S. Ansell, S. Antony, O. Arnold, A. Bekasovs, J. Bilheux, J. Borreguero, K. Brown, A. Buts, S. Campbell, D. Champion, L. Chapon, M. Clarke, S. Cottrell, R. Dalglish, D. Dillow, M. Doucet, N. Draper, R. Fowler, M. A. Gigg, G. Granroth, M. Hagen, W. Heller, A. Hillier, S. Howells, S. Jackson, D. Kachere, M. Koennecke, C. Le Bourlot, R. Leal, V. Lynch, P. Manuel, A. Markvardsen, R. McGreevy, D. Mikkelson, R. Mikkelson, R. Miller, S. Nagella, T. Nielsen, K. Palmen, P. G. Parker, M. Pascal, G. Passos, T. Perring, P. F. Peterson, F. Pratt, T. Proffen, P. Radaelli, J. Rainey, S. Ren, M. Reuter, L. Sastry, A. Savici, J. Taylor, R. J. Taylor, M. Thomas, R. Tolchenov, R. Whitley, M. Whitty, S. Williams, W. Zhou, and J. Zikovsky, *Mantid: Manipulation and analysis toolkit for instrument data.* (2013).
- [75] R. Applin, R. Baust, A. Diaz-Alvarez, C. Finn, S. Foxley, J. Haigh, T. Hampson, and P. F. Peterson, *Mantid 6.9.1: Manipulation and analysis toolkit for instrument data.* (2024).
- [76] B. H. Toby and R. B. Von Dreele, *Journal of Applied Crystallography* **46**, 544–549 (2013).
- [77] S. F. Mughabghab, in *Atlas of Neutron Resonances* (Elsevier, 2018) pp. 1–16.
- [78] Thermal neutron resonances — ncnr.nist.gov, <https://www.ncnr.nist.gov/resources/activation/resonance.html>, [Accessed 14-11-2024].
- [79] Bruker-AXS. APEX3, Madison, WI, USA (2016).
- [80] L. Krause, R. Herbst-Irmer, and D. Stalke, *Journal of Applied Crystallography* **48**, 1907–1913 (2015).
- [81] G. M. Sheldrick, *Acta Crystallographica Section A Foundations and Advances* **71**, 3–8 (2015).
- [82] G. M. Sheldrick, *Acta Crystallographica Section C Structural Chemistry* **71**, 3–8 (2015).
- [83] H. D. Flack, *Acta Crystallographica Section A* **39**, 876 (1983).
- [84] F. Wöhler and H. S. Deville, *Justus Liebigs Annalen der Chemie* **101**, 347–355 (1857).
- [85] P. C. Canfield and Z. Fisk, *Philosophical Magazine B* **65**, 1117–1123 (1992).
- [86] A. Valentín-Pérez, P. Rosa, E. A. Hillard, and M. Giorgi, *Chirality* **34**, 163 (2021).
- [87] S. Parsons, *Tetrahedron: Asymmetry* **28**, 1304–1313 (2017).
- [88] H. Flandorfer, D. Kaczorowski, J. Gröbner, P. Rogl, R. Wouters, C. Godart, and A. Kostikas, *Journal of Solid State Chemistry* **137**, 191–205 (1998).

Structural characterization of the candidate Weyl semimetal CeGaGe - Supplementary Information

Liam J. Scanlon,¹ Santosh Bhusal,¹ Christina M. Hoffmann,² Helen He,² Sean R. Parkin,³ Brennan J. Arnold,¹ and William J. Gannon¹

¹Department of Physics and Astronomy, University of Kentucky, Lexington, KY 40506 USA

²Neutron Scattering Division, Oak Ridge National Laboratory, Oak Ridge, TN 37831 USA

³Department of Chemistry, University of Kentucky, Lexington, KY 40506 USA

(Dated: December 9, 2024)

I. Energy Dispersive X-Ray Spectroscopy

An optical image and several scanning electron images of the sample used for single crystal neutron diffraction (SNCD) can be seen in Fig. S-1. The optical image (Fig. S-1(a)) shows the relative scale of the sample used in the neutron diffraction experiment. The scanning electron images of three different areas of the sample (Fig. S-1(b-d)) show the sample surface in more detail. White boxes in the scanning electron images mark all 38 sites where energy dispersive x-ray spectroscopy (EDX) data were taken. A representative EDX spectrum is shown in Fig. S-2. The fit to the EDX spectrum includes the pulse pileup correction, so photon counts that overlap in time can be resolved individually [1]. The fit matches the data well. When oxygen is included in the stoichiometric calculation, the average oxygen content is 15.67% with a standard deviation of 11.51% for all 38 sites. As there is no evidence of any oxide in any of the diffraction experiments conducted on these samples, this indicates that the oxygen present in the EDX spectra is residual oxygen in the SEM chamber. Uncertainty values for EDX were found by taking the standard deviation of the compositions found at 38 sites on the sample.

II. Powder X-Ray Diffraction

The refined crystallographic parameters for both the $I4_1md$ and $I4_1/amd$ structural models from powder x-ray diffraction (PXR) measurements can be seen in table S-I. The constraint that the fractional z -coordinates of Ga and Ge add to 1 in the $I4_1md$ structure was lifted, resulting in the fractional z -coordinates

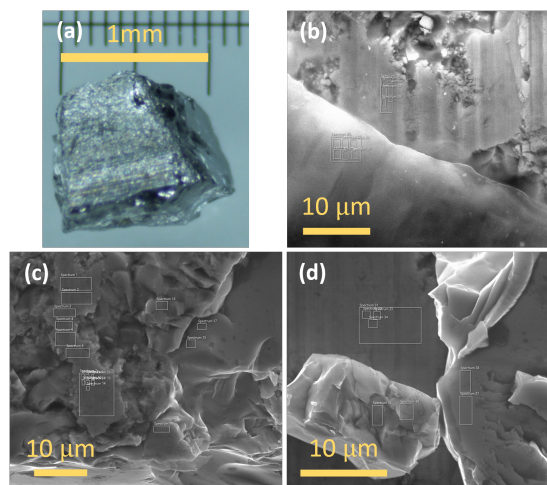


FIG. S-1. Images of the CeGaGe sample used for SNCD: (a) Optical image of the sample. (b-d) Scanning electron images of the sample from the Quanta FEI electron microscope. In each image, the faint white boxes indicate the sites where EDX data were taken.

summing to 0.996(2). When a SCND refinement with $I4_1md$ symmetry was carried out without this constraint, the z -coordinates added to 0.999(1). From the SCND refinement, it was concluded that the z -coordinates very likely add to 1 and the discrepancy from this in the refinement was an artifact of numerical minimization and so a refinement with the z -coordinate constraint is reported in the main text. Given table S-I, the reliability factors and goodness of fit values reported in the main text, and Fig. 2 in the main text, it can be seen that the PXR refinements do not distinguish between the two space groups.

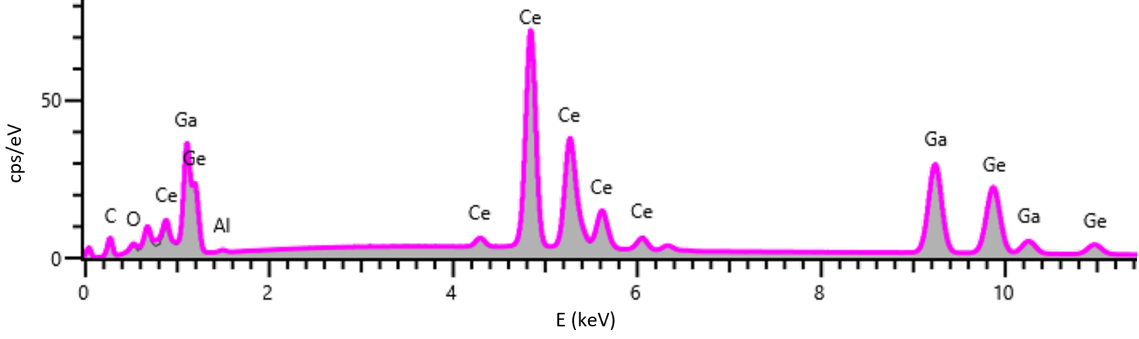


FIG. S-2. Representative EDX spectrum for CeGaGe. The gray, solid region represents the data and the pink curve represents a fit to the data with pulse pileup correction [1]. The elements responsible for the main transitions observed are labeled.

	a [Å]	c [Å]	V [Å ³]
$I4_1md$	4.27503(2)	14.5700(1)	266.280(3)
$I4_1/amd$	4.27505(2)	14.5700(1)	266.283(3)

	Atom	x	y	z	occ.
$I4_1md$	Ce	0.0	0.0	0.000	1.00
$I4_1/amd$	Ce	0.0	0.0	0.000	1.00
$I4_1md$	Ga	0.0	0.0	0.4155(9)	1.00
$I4_1/amd$	Ga	0.0	0.0	0.4177(1)	0.50
$I4_1md$	Ge	0.0	0.0	0.5803(8)	1.00
$I4_1/amd$	Ge	0.0	0.0	0.4177(1)	0.50

TABLE S-I. Crystallographic information of the CeGaGe structure using both $I4_1md$ and $I4_1/amd$ symmetries in PXRD refinements. The crystallographic axes of the two space group refinements are within uncertainty of each other and atomic coordinates match to two significant figures.

III. Single Crystal X-Ray Diffraction

Crystallographic parameters for the structure of the zone refined sample used for SCND, determined by single crystal x-ray diffraction (SCXRD) at 100 K, are summarized in Table S-II. SCXRD measurements were made on a crystal grown with the flux technique at both room temperature and at $T = 100$ K. There is

	a [Å]	c [Å]	V [Å ³]
$I4_1md$	4.2673(1)	14.5413(4)	264.80(1)
$I4_1/amd$	4.2752(1)	14.4999(6)	265.02(2)

	Atom	x	y	z	occ.
$I4_1md$	Ce	0.0	0.0	0.0	1.00
$I4_1/amd$	Ce	0.0	0.0	0.0000	1.00
$I4_1md$	Ga	0.0	0.0	0.4159(1)	1.00
$I4_1/amd$	Ga	0.0	0.0	0.417(2)	0.50
$I4_1md$	Ge	0.0	0.0	0.5825(1)	1.00
$I4_1/amd$	Ge	0.0	0.0	0.417(2)	0.50

TABLE S-II. Crystallographic information of the CeGaGe structure using both $I4_1md$ and $I4_1/amd$ symmetries in SCXRD refinements. The crystallographic axes of the two space group refinements match to two significant figures and the atomic coordinates match to two significant figures.

a subtle, but clear structural transition that is observed in the flux-grown sample, as described in the main text. A refinement of the 100 K SCXRD data for this sample was carried out using $P4_3$ symmetry (space group 78). The crystallographic information for this refinement is in table S-III.

IV. Verifying SCND data quality

In addition to Fig. 3 in the main text, Fig. S-3 shows two other reciprocal space planes to

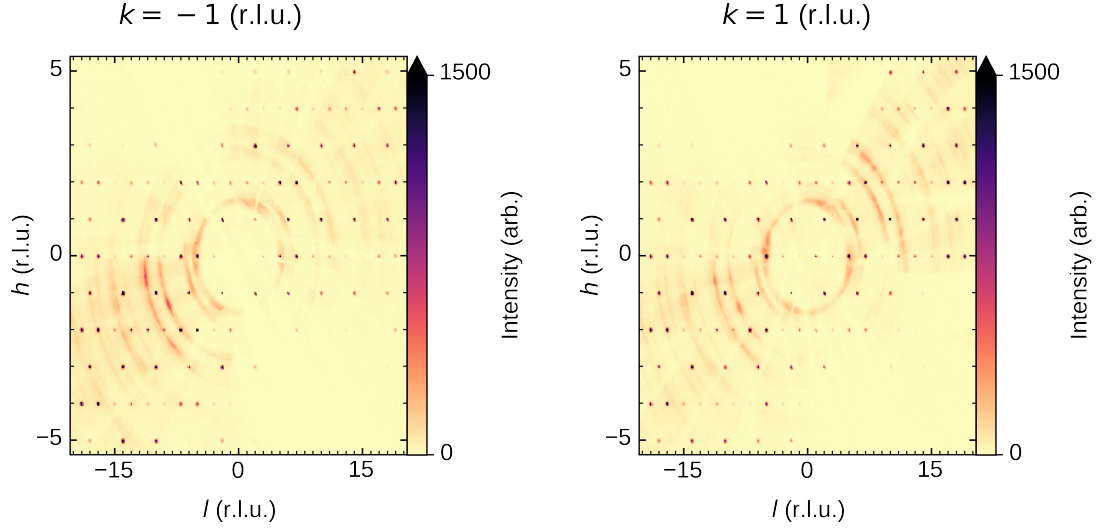


FIG. S-3. Plots of merged SCND data in the $k = \pm 1$ plane. Data for the 19 different goniometer angles merged well and sample is single crystalline.

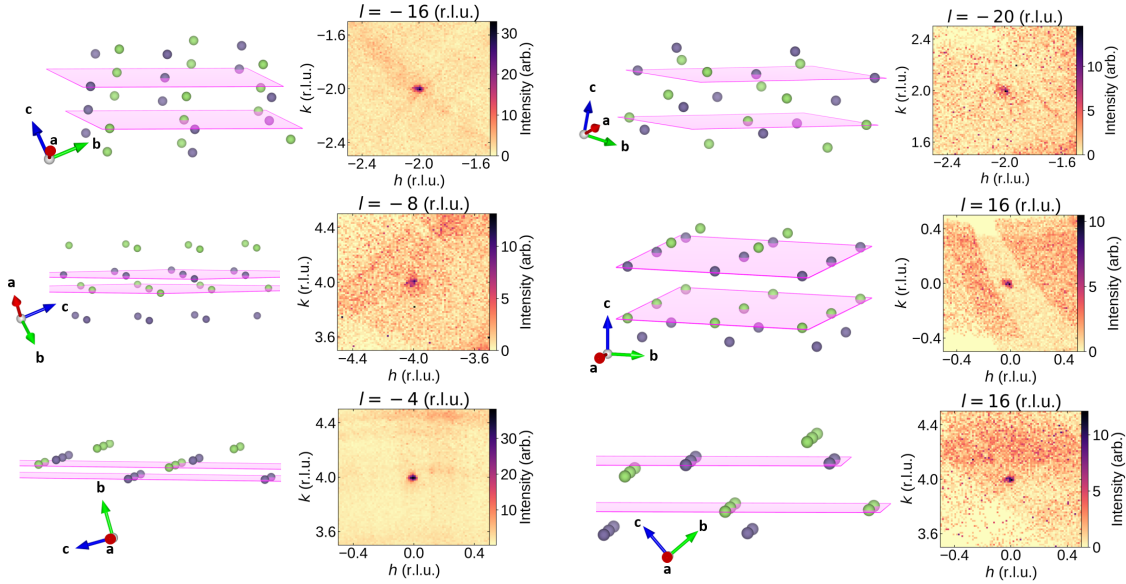


FIG. S-4. Six examples, including the peak from Fig. 6 in the main text, where $10^{-4} \leq |F_c|^2 \leq 1.21$ in Fig. 4(d) of the main text and the discrepancy between space groups $I4_1md$ and $I4_1/amd$ is most pronounced. In each case, the corresponding Bragg planes for space group $I4_1md$ can contain Ga with no Ge or vice versa.

a [Å]	c [Å]	V [Å ³]
4.2756(1)	14.5414(3)	265.83(1)

Atom	x	y	z	occ.
Ce	0.24849(8)	0.25156(8)	0.66595(9)	1.00
Ga	0.2530(2)	0.7297(3)	0.50001(4)	1.00
Ge	0.2297(3)	0.7531(2)	0.33335(4)	1.00

TABLE S-III. Crystallographic information of the CeGaGe structure for $P4_3$ single crystal XRD refinements.

demonstrate that the data for all 19 ϕ angles have merged well and that single Bragg peaks are seen at integer coordinates in reciprocal space. The only other features that are seen in Fig. S-3 and Fig. 3 in the main text are powder scattering rings from the aluminum present in the sample holder, sample environment, and instrument windows.

V. Quality of data where $10^{-4} \leq |F_c|^2 \leq 1.25$

Fig. S-4 shows 6 examples from the 1236 data points from figure 5 in the main text that give the strongest determination between the noncentrosymmetric $I4_1md$ symmetry, and centrosymmetric $I4_1/amd$ symmetry.

A defining feature of the 6 example peaks in Fig. S-4 is that the Bragg planes can have Ga atoms with no Ge atoms or vice versa. Considering planes of pure Ga or Ge for $I4_1md$ sym-

metry, versus planes of mixed Ga and Ge for $I4_1/amd$ symmetry gives intuition as to why these structure factors for the $I4_1/amd$ symmetry would be significantly lower.

It can be shown mathematically that the Bragg planes can contain Ga with no Ge or vice versa for each of the reflections shown in Fig. S-4. Let \vec{b}_1 be the atomic basis vector of a Ga atom in a Bragg plane with indices h, k, l . Let \vec{b}_2 represent any of the atomic basis vectors of Ge. Let \vec{u} be the reciprocal lattice vector corresponding to the Bragg plane and \vec{v} represent any Bravais lattice vector of the crystal. The condition for a Bragg plane to contain Ga but no Ge is

$$\vec{u} \cdot \vec{b}_1 \neq \vec{u} \cdot (\vec{b}_2 + \vec{v}) \quad (\text{S-1})$$

for any \vec{b}_2 and any \vec{v} . If \vec{u} is expressed in terms of reciprocal lattice vectors and $\vec{v}, \vec{b}_1, \vec{b}_2$ are expressed in terms of direct lattice vectors, $\vec{u} \cdot \vec{v}$ can be any integer obtainable by integer combination of $h, k,$ and l , so the condition for a Bragg plane to contain Ga but no Ge is

$$\vec{u} \cdot (\vec{b}_1 - \vec{b}_2) \neq n \quad (\text{S-2})$$

where n is, using Bezout's identity, any nonzero multiple of the greatest common divisor of $h, k,$ and l .

Computations were carried out for each reflection in Fig. 5 in the main text to verify that corresponding Bragg planes contain Ga with no Ge or vice versa.

[1] P. Statham, *Microscopy and Microanalysis* **13**, 1428 (2007),

<https://academic.oup.com/mam/article-pdf/13/S02/1428/48134251/mam1428.pdf>.